Dynamics of the West African Westerly Jet

BING PU

Department of Earth and Atmospheric Sciences, Cornell University, Ithaca, New York

KERRY H. COOK

Department of Earth and Atmospheric Sciences, Cornell University, Ithaca, New York, and Department of Geological Sciences, Jackson School of Geosciences, The University of Texas at Austin, Austin, Texas

(Manuscript received 1 February 2010, in final form 10 August 2010)

ABSTRACT

The West African westerly jet (WAWJ) is a low-level westerly jet located at 8°–11°N over the eastern Atlantic and the West African coast. It is clearly distinguished from the monsoon westerly flow by its structure and dynamics, and plays an important role in transporting moisture from the tropical eastern Atlantic to Sahelian West Africa during boreal summer.

The WAWJ develops in early June, sustains maximum wind speeds of 5–6 m s^{-1} from late July to early September, and weakens and dissipates by mid-October. In its mature stage, the WAWJ is located within the Atlantic ITCZ. It extends from the surface to 700 hPa, with maximum speed at 925 hPa. The jet has a weak semidiurnal cycle, with maxima at 0500 and 1700 local time.

A momentum budget analysis reveals that the WAWJ forms when a region of strong westerly acceleration is generated by the superposition of the Atlantic ITCZ and the westward extension of the continental thermal low. The WAWJ is supergeostrophic at its maximum, with zonal pressure gradient and Coriolis accelerations both pointing eastward. While much of the WAWJ's seasonal variation can be explained by the geostrophic wind, the ageostrophic wind contributes more than 40% of the wind speed during the jet's formation and demise.

The westward extension of the thermal low is associated with the formation of an offshore low, which is related to seasonal warming of the ocean between 6° and 18°N along the coast. The coastal SSTs vary in response to a net surface heating pattern with warming to the north and cooling to the south, which is mainly controlled by solar radiative and latent heat fluxes.

1. Introduction

It has long been recognized that the eastern tropical Atlantic is an important moisture source for West Africa, and that low-level westerlies transport moisture onto the continent in boreal summer (Lamb 1983; Koster et al. 1986; Cadet and Nnoli 1987; Druyan and Koster 1989; Grist and Nicholson 2001; Fontaine et al. 2003). The westerly flow near 10°N along the West African coast was identified as a jet in satellite-based observations by Grodsky et al. (2003). Here we refer to this feature as the West African westerly jet (WAWJ), and study its dynamics.

West Africa is known to have especially strong atmosphere–ocean–land surface interactions. The association between the WAWJ and moisture transport onto the continent suggests that the jet plays an important role in the coupled system. In this paper we investigate the basic dynamics of the WAWJ's formation and maintenance. The jet's climatological structure, seasonality, and diurnal cycle are documented, and the processes that cause it to form and persist are investigated. In particular, we clearly distinguish the WAWJ from the westerly monsoon flow.

Studies of the low-level westerly flow over West Africa are reviewed in the following section. Section 3 is a description of the datasets and methods used to investigate the WAWJ dynamics. In section 4, climatological features of the WAWJ in the reanalyses are presented, and the jet dynamics is diagnosed in section 5. The last section contains the main conclusions.

2. Background

Low-level jets are known to be important sources of moisture for low-latitude precipitation systems. They

Corresponding author address: Bing Pu, Dept. of Earth and Atmospheric Sciences, Cornell University, Ithaca, NY 14853.
E-mail: bp247@cornell.edu

DOI: 10.1175/2010JCLI3648.1

are often related to orographic features, such as the Great Plains, South American, and Somali low-level jets, but not necessarily, as in the Caribbean low-level jet.

Based on the Quick Scatterometer (QuikSCAT) wind data, Grodsky et al. (2003) find that the surface westerlies embedded within the Atlantic ITCZ at about 7°–12°N near the West African coast form a jet that persists from May to September, with a maximum wind speed exceeding 7 m s^{-1} in late boreal summer. In strong jet years, such as 1999, they report surface westerly wind speeds in excess of 15 m s^{-1} at some locations. Grodsky et al. (2003) find that a linear three-term (pressure gradient, Rayleigh friction, and Coriolis force) momentum balance provides a reasonable description of the zonal winds. They conclude that the jet is in near-geostrophic balance, and the meridional pressure gradient is generated by a westward extension of the continental thermal low over the eastern Atlantic.

Grodsky et al. (2003) also discuss how the ocean responds to the WAWJ. They find that both observations and GCM simulations suggest that the jet cools the SST by ~0.3 K through entrainment and latent heat loss. The Ekman pumping associated with the jet causes cooling and shallowing of the ocean mixed layer to the north and warming and deepening to the south. The resulting strengthened meridional gradient of sea surface height between 10°N and the equator could intensify the North Equatorial Counter Current transport by 15%.

Several factors inspired us to pursue further study of the WAWJ. One is results from a study of the African humid period (AHP), which occurred 6000–8000 years ago at a time of high surface moisture across the Sahel and Sahara caused by greater summertime insolation. Atmospheric GCMs typically underpredict AHP rainfall (Braconnot et al. 2000). Patricola and Cook (2007) used a regional climate model (atmosphere only) to show that one can capture a reasonable simulation of the AHP if the changed conditions of the land surface (most notably soil moisture) are specified in the model in addition to the increased summer insolation. The monsoon flow across the Guinean coast does not change between the present day and AHP simulations, but the WAWJ strengthens and deepens considerably and is the primary source of moisture for the northward expansion of the monsoon. This response, combined with the elimination of the African easterly jet along with its role in transporting moisture off the continent (Cook 1999), explains the increased wetness of the AHP climate. The failure of coarser-resolution models to resolve this jet may be one reason atmospheric GCMs underpredict AHP rainfall.

Another regional modeling study also exposed a crucial role for the WAWJ in West African climate change and variability. Patricola and Cook (2008) used a coupled atmosphere–vegetation regional model to generalize the results from the AHP study described above and understand the implications for potential abrupt climate change over northern Africa. Idealized simulations were conducted to test the dependence of the northern Africa climate on the initial conditions specified for vegetation. When the coupled model is initialized with the Sahara desert border placed anywhere south of 17.9°N, the coupled model equilibrates to a climate similar to today's climate. In contrast, when the coupled model is initialized with the Sahara border at or north of 17.9°N, a ''green Sahara'' solution results. This green Sahara solution occurs because the initial conditions place higher levels of soil moisture at the latitude of the thermal low. Initially fueled by moisture evaporated from the surface, the thermal low deepens and replaces the dry, shallow thermal low–Saharan high system of the present day climate. Again, the WAWJ is the agent that sustains a strong moisture flux into northern Africa; the southerly monsoon flow across the Guinean coast is unchanged.

These studies demonstrate that the westerly flow onto the continent—nominally the WAWJ—can vary independently of the southwesterly monsoon flow. There are two distinct low-level westerly flow regimes important for transporting moisture to the West African continent in summer months. One is the westerly component of the monsoon flow, which results from the Coriolis acceleration acting on the southerly flow across the Guinean coast driven most fundamentally by land–sea contrast. The other is the WAWJ.

Previous studies have examined the westerly flow onto northern African's west coast and documented its importance in bringing moisture onto the African continent without identifying the flow as a jet. Gu and Adler (2004) find that the formation of strong low-level westerly flow between 10°W and 10°E at 850 hPa is coincident with the development of rain along 10°N over West Africa in June and July. During boreal summer, when moisture transport from the Gulf of Guinea is reduced because of the development of the Atlantic cold tongue, transport by westerly winds can be very important. Sijikumar et al. (2006) find that both in a regional model and the 40-yr European Centre for Medium-Range Weather Forecasts (ECMWF) Re-Analysis (ERA-40) reanalysis the onset of the West African monsoon is characterized by an enhanced westerly flow at 10°–15°N between the eastern Atlantic and the continent.

Previous studies also demonstrate the importance of the westerly flow in the region's variability, but without distinguishing between the WAWJ and the monsoon westerlies. Grist and Nicholson (2001) find differences in the westerly flow between 10°W and 20°E between wet and dry years in the Sahel, with westerly flow anomalously

strong and deep during wet years. Nicholson and Grist (2003) suggest that the westerlies are best developed from July through September, especially between 10°W and 10°E in association with Coriolis acceleration of the southeasterly trades. Tomas and Webster (1997) indicate that inertial instability adds to this westerly acceleration. Jury et al. (2002) demonstrate a link between the zonal wind in the central Atlantic (10°S–5°N, 40°W–0°) and African rainfall. Fontaine et al. (2003) find that the near surface (1000–925 hPa) westerly moisture flux is enhanced in wet years. Using a regional climate model, Hagos and Cook (2008) find that, in response to Atlantic and Indian Ocean warming in the 1990s, anomalous westerly flow brings moisture onto the West African continent to support the Sahel rainfall recovery of that period.

In summary, previous work suggests that this small feature, the WAWJ, is important for understanding climate—including its variability and change—in Sahelian Africa.

3. Methodology

The 6-hourly ERA-40 reanalysis (Uppala et al. 2005; data available online at http://dss.ucar.edu/datasets/ds127.1/ and http://dss.ucar.edu/datasets/ds127.0/) at T106 resolution (equivalent to about 1.125° latitude by 1.125° longitude on the Gaussian grid) from 1958 to August 2002 is used to create the climatological daily and 6-hourly variables used in this study. This reanalysis is chosen as the primary source because of its relatively high spatial resolution and long time coverage. We choose not to extend the analysis past August 2002 because the ERA-40 reanalysis is sufficiently long to provide a climatology. This is preferable in order to avoid issues that would arise if we extended the record by matching with a different reanalysis.

In regions with a sparse observing network such as West Africa, any reanalysis product relies heavily on model simulation. So we also compare the ERA-40 reanalysis to the monthly National Centers for Environmental Prediction (NCEP)/National Center for Atmospheric Research (NCAR) reanalysis (NCEP1; Kalnay et al. 1996) from 1958 to 2001 and the NCEP/Department of Energy (DOE) Atmospheric Model Intercomparison Project (AMIP-II) reanalysis (NCEP2; Kanamitsu et al. 2002) daily reanalysis from 1979 to 2001. These products have a coarser resolution than the ERA-40 reanalysis, at 2.5° latitude and longitude. Since satellite observations are not available before 1979, we compared the jet climatologies for 1958–78 and 1979–2001. For the years after 2001, we also examined the ERA-Interim reanalysis climatology (Simmons et al. 2007a,b) for 1989–2008 and the ECMWF African Monsoon Multidisciplinary Analysis (AMMA) operational analysis climatology (http://bddamma.ipsl.polytechnique.fr/available-datasets-4.html) for 1999–2007.

The QuikSCAT SeaWind observations used by Grodsky et al. (2003) have higher resolution (25 km by 25 km) than the ERA-40 reanalysis. However, the time coverage of this wind dataset is shorter (June 1999–present) and is, therefore, not suitable for a study of the climatological jet.

To understand the formation and maintenance of the WAWJ, terms in the horizontal momentum balance are analyzed in the following vector form:

$$\frac{d\mathbf{V}}{dt} = -\nabla\Phi - f\mathbf{k}\times\mathbf{V} + \mathbf{F}_h, \tag{1}$$

where the Lagrangian acceleration is defined by

$$\frac{d}{dt} = \left(\frac{\partial}{\partial t}\right)_p + \left(u\frac{\partial}{\partial x} + v\frac{\partial}{\partial y}\right)_p + \omega\frac{\partial}{\partial p}; \tag{2}$$

$\mathbf{V} \equiv (u, v)$ is the horizontal velocity vector, in which u is the zonal wind and v is the meridional wind. Also, ω is the vertical p-velocity. The first term on the right-hand side of Eq. (1) is the acceleration due to horizontal geopotential height gradients, where Φ is geopotential height. The second term is the horizontal Coriolis acceleration, where $f \equiv 2\Omega\sin\phi$ is the Coriolis parameter, Ω is the angular speed of rotation of the earth $= 7.292 \times 10^{-5}$ rad s^{-1}, and ϕ is latitude. The third term represents horizontal friction, which is calculated as a residual in the analysis and so contains error due to the estimation of derivatives by finite differencing.

The component equations of Eq. (1) are also used in the analysis as follows:

$$\frac{du}{dt} = -\frac{\partial\Phi}{\partial x} + fv + R_x \tag{3}$$

and

$$\frac{dv}{dt} = -\frac{\partial\Phi}{\partial y} - fu + R_y, \tag{4}$$

where R_x and R_y are the residual terms mentioned above.

The ageostrophic zonal wind is also examined, defined by

$$u_a = u - u_g = u + \frac{1}{f}\frac{\partial\Phi}{\partial y} = -\frac{1}{f}\left(\frac{dv}{dt} - R_y\right). \tag{5}$$

The 6-hourly ERA-40 reanalysis and forecast surface variables are used to derive climatological (1958–2001) daily values for the surface heat budget analysis in section 5.

Assuming that there are no horizontal or vertical heat fluxes out of or into the atmosphere–ocean column, the net surface heating is calculated based on the following equation:

$$Q_{\text{net}} = Q_{\text{sw}} + Q_{\text{lw}} + Q_{\text{sh}} + Q_{\text{lh}}, \tag{6}$$

where Q_{net} is the net surface heating, and Q_{sw}, Q_{lw}, Q_{sh}, and Q_{lh} are the net downward solar radiation, net upward longwave radiation, upward sensible heat flux, and upward latent heat flux, respectively.

4. The WAWJ in the reanalyses

Figures 1a,b display the 1958–2001 July–September climatology of winds and geopotential heights at 925 hPa over West Africa in the ERA-40 and NCEP1 reanalyses, respectively. In the ERA-40 reanalysis (Fig. 1a), the WAWJ is located off the west coast of Africa between 8° and 11°N, clearly distinguished from the southwesterly monsoon flow maximum over the continent between 0° and 5°E. The jet is not well captured in the lower-resolution NCEP1 reanalysis (Fig. 1b), but the two reanalysis products are in general agreement about the large-scale flow and geopotential height distribution. An examination of the other reanalysis products listed in section 3 also produce WAWJ features that are consistent with those in the ERA-40 climatology (not shown), justifying the use of the ERA-40 reanalysis for this investigation.

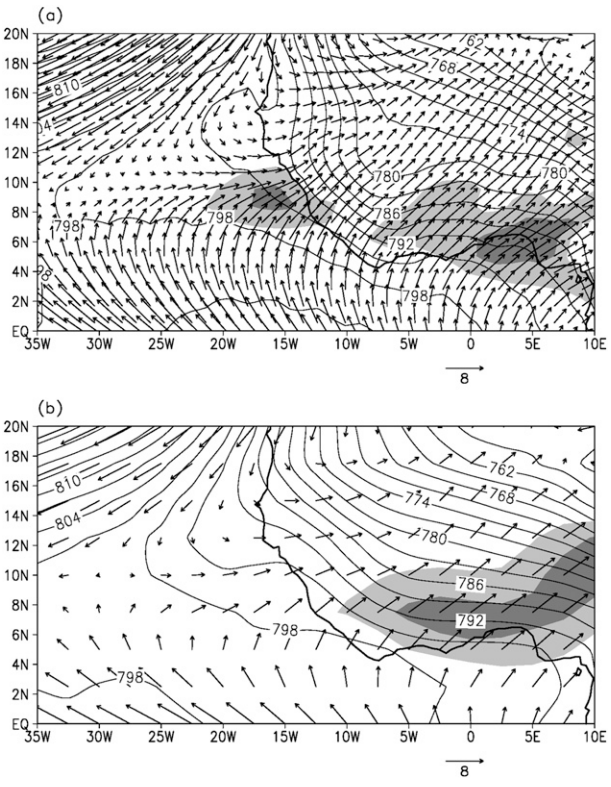

FIG. 1. The 925-hPa winds (m s^{-1}) and geopotential heights (gpm) in the (a) ERA-40 and (b) NCEP1 reanalysis climatologies (1958–2001), averaged from July to September. Zonal wind speeds above 4 m s^{-1} are shaded with light gray, and above 5 m s^{-1} with dark gray. Contour intervals are 3 gpm.

Daily climatological variables are used to study the structure and seasonal cycle of the WAWJ. Based on zonal wind velocities at 925 hPa between 8° and 11°N off the west coast, five stages of jet development are defined. In stages 1 and 5, when the jet forms and terminates, the core zonal wind speed is between 1.5 and 3 m s^{-1}. In stages 2 and 4, when the jet intensifies and weakens, the zonal wind is between 3 and 5 m s^{-1}, and in stage 3, when the jet reaches its maximum, the westerly wind is greater than 5 m s^{-1}. Figures 2a–e display wind vectors, zonal wind shading, and geopotential height contours for each stage.

Stage 1 (Fig. 2a) lasts from 7 to 27 June. Westerly winds develop in the jet region during this stage, with flow down the geopotential height gradient toward land. From 28 to 21 July (defined as stage 2), the low-level jet intensifies. As shown in Fig. 2b, the thermal low (e.g., the 800-gpm contour) extends westward over the ocean during this time. This forms an offshore low (marked with an ''X''), which is related to the dynamics of the jet formation discussed below. Note that there is evidence of the low's formation as a region of offshore cyclonic winds in stage 1 (Fig. 2a). The WAWJ extends westward to 22°W and strengthens, with a zonal wind maximum of 4 m s^{-1} at 8°–10°N. Over land, the zonal wind at 14°–18°N is also stronger than in stage 1 as the monsoon flow expands northward to about 19°N over West Africa.

The jet reaches peak intensity in stage 3 (Fig. 2c). From 22 July until 5 September, it extends from 13° to 30°W, and the offshore low extends to about 34°W. At 8°–10°N, zonal wind speeds reach 5 m s^{-1}. When the jet expands eastward across the coast, the winds become northwesterly, pointing down the geopotential height gradient toward the continental thermal low.

In stage 4 (Fig. 2d), from 6 to 19 September, the westerly jet weakens to about 4 m s^{-1}, and the offshore low moves southward to 8°–14°N. The jet dissipates in stage 5 (Fig. 2e). From 20 September to 18 October, the westerly winds over the ocean diminish to 1–2 m s^{-1} and the low moves southward to 5°–10°N.

Figure 3a displays a latitude–height cross section of the zonal wind speed averaged from 15° to 25°W during the jet maximum (stage 3). The jet core is located at 925 hPa between 8° and 10°N. Westerly flow extends up to 700 hPa, embedded in the large-scale easterlies. The

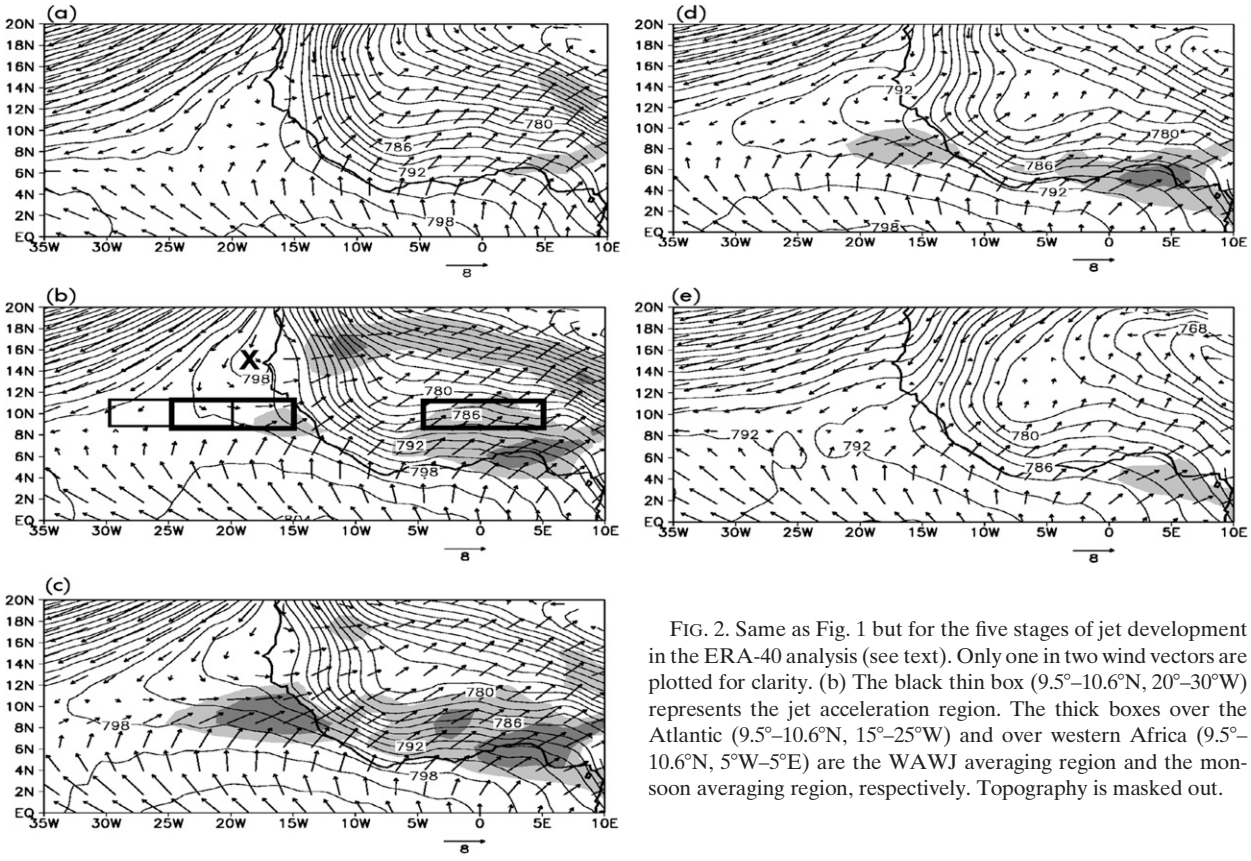

FIG. 2. Same as Fig. 1 but for the five stages of jet development in the ERA-40 analysis (see text). Only one in two wind vectors are plotted for clarity. (b) The black thin box (9.5°–10.6°N, 20°–30°W) represents the jet acceleration region. The thick boxes over the Atlantic (9.5°–10.6°N, 15°–25°W) and over western Africa (9.5°–10.6°N, 5°W–5°E) are the WAWJ averaging region and the monsoon averaging region, respectively. Topography is masked out.

African easterly jet core is located above (600–700 hPa) and north (17°N) of the WAWJ. The tropical easterly jet core is located to the south, near 5°N, at about 250 hPa.

Figure 3b shows a longitude–height cross section at 9.5°N, also for stage 3. (Note that the streamlines intersect the 1000-hPa surface vertically in both Figs. 3a,b in regions with relatively strong vertical velocity because of the 10^3 scaling used. The physical surface over the ocean is at about 1013–1014 hPa.) Below about 750 hPa, the flow is mostly westerly from 35°W to 20°E. The WAWJ maximum is located between 15° and 18°W, with a magnitude of 6 m s^{-1} at 925 hPa. Again, the WAWJ is distinguished from the maxima in the westerly flow over land, which is located at 2°W and 6°–15°E between 900 and 800 hPa.

Compared with the results of Grodsky et al. (2003), the monthly mean westerly wind speed in the jet region is 1 m s^{-1} weaker in the ERA-40 reanalysis climatology. This may be due to the lower resolution of the ERA-40 reanalysis compared with the QuikSCAT data, or to differences in the averaging periods.

To understand the diurnal and seasonal cycles of the WAWJ and compare them with the monsoon flow, two averaging regions are chosen. For the WAWJ, the averaging region is 9.5°–10.6°N and 15°–25°W, and for the monsoon region it is 9.5°–10.6°N and 5°W–5°E (see Fig. 2b). The averaging region for the WAWJ was chosen as the area over which the jet is best defined as purely westerly, and it captures the maximum westerly wind speed. The averaging region for the monsoon flow is located over the same latitude range, and has the same longitudinal extent centered on the Greenwich meridian. A ''jet acceleration'' region to the west of the jet maximum is also defined (9.5°–10.6°N, 20°–30°W). The results presented below are not strongly dependent on the exact location of the averaging regions.

Figure 4 displays climatological 6-hourly zonal wind speeds in the WAWJ (solid line) and the monsoon (dashed line) regions for stage 3. The WAWJ has a weak semidiurnal cycle, with two daily maxima at 0600 and 1800 UTC (0500 and 1700 local time). It is a little stronger at 1800 UTC with a wind speed of about 5 m s^{-1}, and weakest at 1200 UTC (1100 local time) with a speed of 4.2 m s^{-1}. The cycle is similar in the other stages. In the monsoon region, the zonal winds have only one maximum each day, about 5.4 m s^{-1} at 0600 local time (LT), and a minimum of 3.7 m s^{-1} at 1800 LT. The wind speed diurnal range in the monsoon region is about twice that in the jet region.

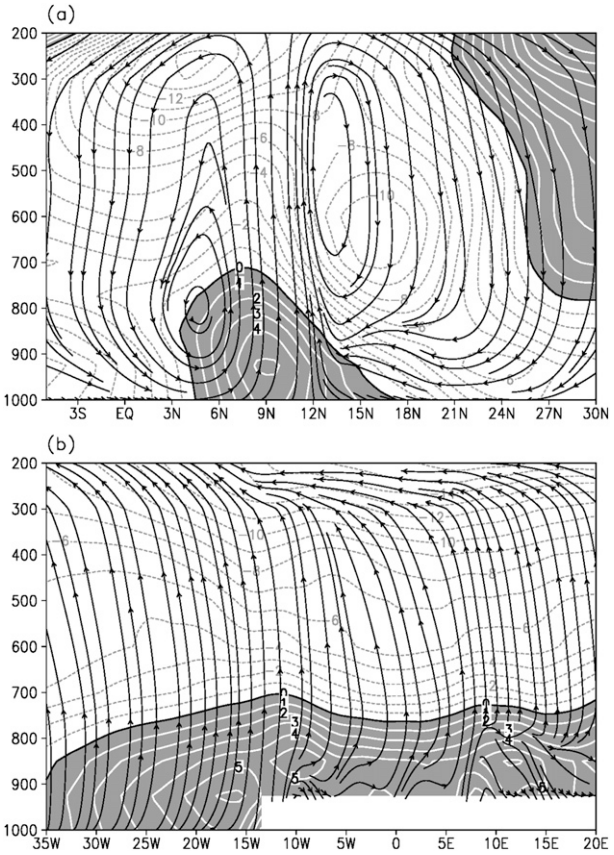

FIG. 3. Cross sections of zonal wind speed (m s^{-1}; westerlies shaded) in the ERA-40 reanalysis with (a) streamlines of meridional and vertical winds (scaled by 10^3) averaged between 15° and 25°W and (b) streamlines of zonal and vertical winds at 9.5°N, averaged from 22 Jul to 5 Sep. Topography is masked out.

The seasonal development of the wind components in the jet region is shown in Fig. 5a. The zonal wind is easterly in May, changes to westerly in early June, maintains a maximum from late July to early September, and returns to easterly in late October. The meridional wind has a similar seasonal cycle to the zonal wind, but the speeds are 3–4 m s^{-1} lower after the WAWJ begins to form. The vertical velocity is relatively strong in the jet region, and it develops rapidly in early summer. These large upward vertical velocities indicate that the WAWJ is collocated with the Atlantic ITCZ, as mentioned by Grodsky et al. (2003).

Figure 5b shows the wind components in the monsoon region. Variations in wind speeds are smaller than in the jet region during the analysis period. The zonal wind remains westerly through almost all of the analysis period, increasing from about 2.5 m s^{-1} in May and June to a maximum of about 5 m s^{-1} from mid-July to mid-August. It peaks about 2 weeks earlier than the WAWJ. The meridional wind is comprised of southerly flow at approximately

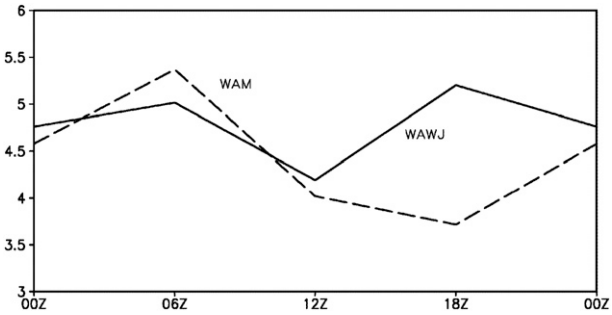

FIG. 4. The 6-hourly zonal wind speeds (m s^{-1}) in the WAWJ (solid) and the West African monsoon (WAM; dashed) averaging regions (see Fig. 2b) in the ERA-40 reanalysis, averaged in stage 3. The time axis is UTC. Local time in the jet region is UTC − 1 h. In the monsoon region, local time is the same as UTC.

4 m s^{-1} throughout the spring and summer, exceeding the zonal wind speed until early July. The vertical velocity in the monsoon region is small throughout the period, further distinguishing the monsoon dynamics from that of the WAWJ. Weak subsidence from May through early June is replaced by essentially zero vertical velocities for the rest of the period.

5. Formation of the WAWJ

a. Dynamics

Tomas and Webster (1997) discuss the mechanisms of low-level tropical westerly flow. They suggest that when the cross-equatorial pressure gradient is large, in the vicinity of the zero absolute vorticity (η) contour, strong zonal wind shear is needed to balance the absolute vorticity advection associated with divergent flow. Therefore, in the Northern Hemisphere, a tropical low-level westerly maximum tends to appear north of the $\eta = 0$ contour. An example of the low-level westerly maximum in the Indian Ocean in boreal summer is displayed to support the argument.

Whether this theory is sufficient to explain the formation of the WAWJ is examined in the ERA-40 reanalysis. Over the eastern Atlantic, the $\eta = 0$ contour is located near 4°N in August, with a maximum zonal wind shear positioned near 4°–5°N (not shown). From 20° to 40°W, westerlies are located to the north of the $\eta = 0$ contour, while easterlies are located to the south. However, the WAWJ is located about 5° farther north of this zonal wind shear maximum, which suggests that the formation of the jet is not only related to the large-scale absolute vorticity advection but also is associated with regional-scale dynamics. Also, as pointed out by Grodsky et al. (2003), this mechanism does not explain the westward extension of the continental thermal low and the southward pressure gradient in the jet region. Here we try to

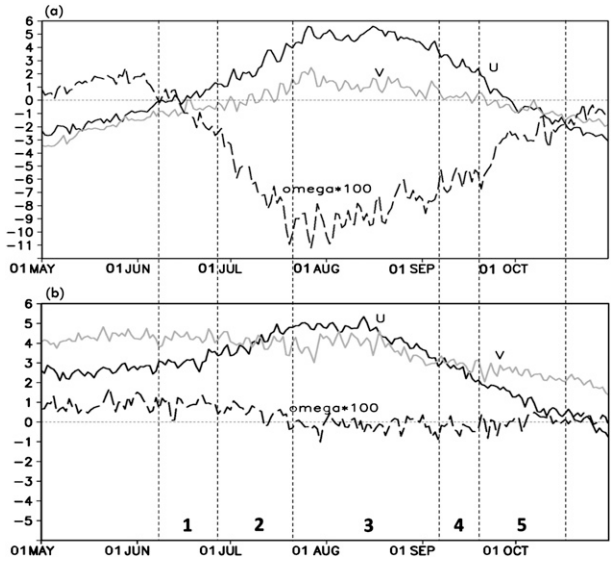

FIG. 5. Averaged wind speeds in the (a) WAWJ (15°–25°W) and (b) monsoon (5°W–5°E) regions at the same latitudes (9.5°–10.6°N) in the ERA-40 reanalysis. The averaging regions are shown in Fig. 2b. Black solid, gray solid, and black dashed lines represent the averaged zonal, meridional (m s^{-1}) and vertical p-velocities (Pa s^{-1}, scaled by 10^2), respectively. The numbers indicate the stages of the WAWJ as defined in Fig. 2.

answer these questions through momentum and surface heat budgets analyses.

Figures 6a–d display the spatial distribution of each term in the vector horizontal momentum equation [Eq. (1)] at the time of the WAWJ maximum (stage 3). The contours and vectors indicate the magnitudes and directions of the forces, respectively.

Within the North Atlantic subtropical high, in the upper left corner of each panel (11°–15°N, 22°–35°W), the flow is essentially geostrophic, with large and opposite pressure gradient (Fig. 6a) and Coriolis terms (Fig. 6b), and small acceleration and friction terms (Figs. 6c,d, respectively).

Further south, over the eastern Atlantic in the vicinity of the WAWJ (7°–11°N, 14°–32°W), pressure gradient forces (Fig. 6a) are directed mainly northward, with a maximum between 8° and 10°N near 20°W, south of the offshore low (Fig. 2b). The Coriolis forces in this region (Fig. 6b) are directed southward and southeastward, with magnitudes 2–3 $\times$ 10^{-5} m s^{-2} greater than the pressure gradient forces. The acceleration term (Fig. 6c) is small in the vicinity of the WAWJ, but south of the jet region the acceleration is greater and aligned with the Coriolis force. The residual term is comparable in magnitude to the acceleration term (Fig. 6d). It opposes the wind direction in general, supporting the interpretation of this term as friction.

Over West Africa, the flow is strongly ageostrophic, with pressure gradient and Coriolis forces essentially perpendicular to each other (Figs. 6a,b). The acceleration term (Fig. 6c) is relatively small. The residual is the largest term, again suggesting that this term reflects frictional accelerations, which are expected to be large in the well-developed planetary boundary layer over tropical land surfaces. The residual term decreases rapidly with elevation (not shown).

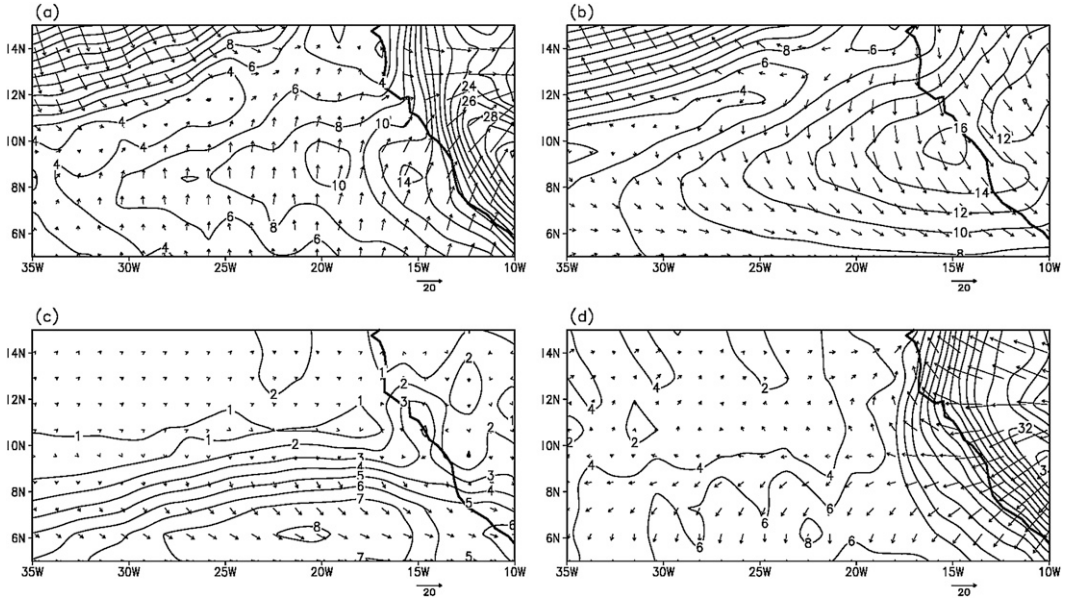

FIG. 6. Vectors representing terms in Eq. (1), with contours showing magnitudes (10^{-5} m s^{-2}), averaged over the jet maximum period, as follows: (a) geopotential height gradient, (b) Coriolis, (c) acceleration, and (d) residual terms.

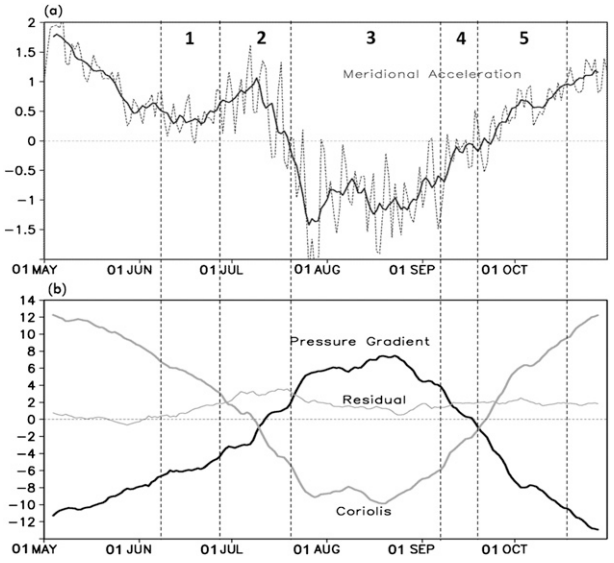

FIG. 7. Meridional momentum budget terms [Eq. (4)] in the jet acceleration region (shown in Fig. 2b), calculated from the ERA-40 reanalysis. (a) Meridional acceleration (black dotted line) with seven-day running mean (black solid line); (b) seven-day running mean of the meridional geopotential height gradient (black thick line), Coriolis (gray thick line), and residual (gray thin line; 10^{-5} m s^{-2}).

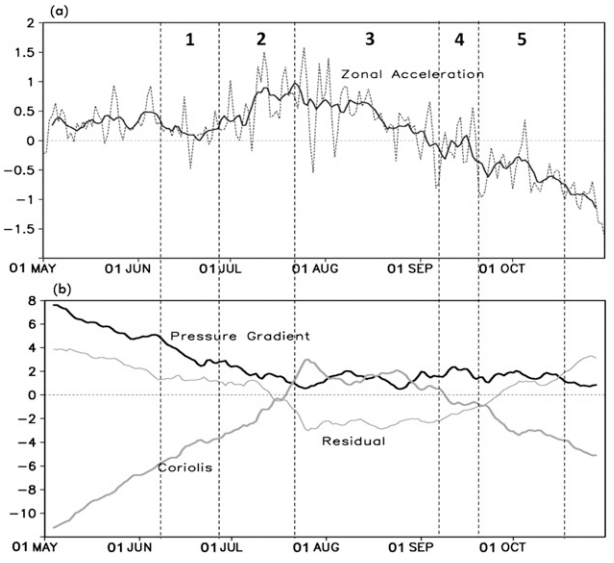

FIG. 8. As in Fig. 7, but for the zonal momentum budget [Eq. (3)].

To understand how the WAWJ forms, the evolution of the momentum balance [Eqs. (3) and (4)] is analyzed in the jet acceleration region (Fig. 2b). The climatological meridional acceleration (dv/dt) is shown by the dotted line in Fig. 7a, with a smoothed version using a seven-day running mean denoted by the black solid line. The numbers in Fig. 7a indicate the stages of the WAWJ as defined in Fig. 2. The meridional acceleration is negative during stage 3, that is, during the maximum of the WAWJ, and positive at all other times.

Each term in the meridional momentum budget [rhs of Eq. (4)] is shown in Fig. 7b. The first-order momentum balance is geostrophic. Negative values of the pressure gradient force before the middle of July are associated with the high to the north of the WAWJ acceleration region. This negative pressure gradient force weakens from May through July as the North Atlantic subtropical high intensifies and shifts northward in its normal seasonal cycle (see Figs. 2a–c). At the same time, the marine ITCZ moves northward in its seasonal cycle. The low-level convergence zone, which moves to about 11°N in the far eastern Atlantic because of the proximity to the continent (Hagos and Cook 2005), becomes collocated with the jet acceleration region in July (Fig. 2c), and the pressure gradient force changes sign (Fig. 7b).

From mid-July to early September, the Coriolis force associated with the high zonal velocities of the WAWJ is approximately 2.5×10^{-5} m s^{-2} greater than the pressure gradient force. Thus, the WAWJ is supergeostrophic when it is mature.

An examination of the u-momentum balance [Eq. (3)] explains the processes that accelerate the flow eastward. The climatological zonal acceleration (du/dt) is shown by the dotted line in Fig. 8a, with a smoothed version using a seven-day running mean denoted by the black solid line. Positive (eastward) acceleration increases by about 1×10^{-5} m s^{-2} from stage 1 to 2, and the westerly wind intensifies. In stage 3, the eastward zonal acceleration weakens after a maximum in late July, and becomes westward in early September. The westward zonal acceleration strengthens through stage 4 (Fig. 2d) and stage 5 (Fig. 2e), and the jet is destroyed.

Each term on the rhs of Eq. (3) is plotted in Fig. 8b. The zonal momentum balance is approximately geostrophic until the middle of July, with opposing pressure gradient and Coriolis forces decreasing in magnitude as the continental thermal low extends westward over the eastern Atlantic (Figs. 2a,b), and with friction supporting the pressure gradient force. After the middle of July, the pressure gradient force settles into a relatively low positive value (about 2×10^{-5} m s^{-2}) as the westward extension of the thermal low becomes established (Fig. 2c). The Coriolis force changes sign at the end of stage 2, and zonal geostrophic balance is interrupted during the jet maximum period (stage 3). This change in the sign of the u-momentum equation Coriolis force; that is, the sign change in v shown in Fig. 5a, occurs as the low-level tropical convergence zone (the marine ITCZ) moves across the jet acceleration region.

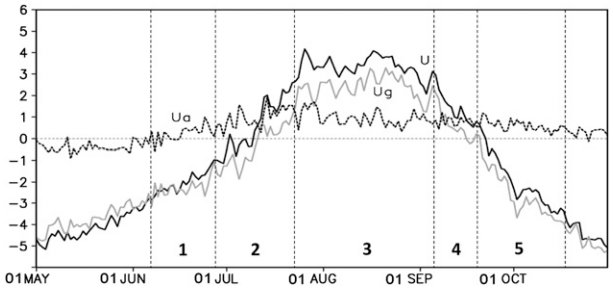

FIG. 9. Zonal geostrophic (gray solid line), ageostrophic (black dashed line), and total wind speeds (black solid line) in the jet acceleration region.

Figure 9 shows the zonal geostrophic and ageostrophic wind components, calculated based on Eq. (5), along with the total wind speed in the jet acceleration region. From early June to mid-July, and from late September to mid-October, the ageostrophic wind is in the opposite direction to the geostrophic wind, since the pressure gradient force ($-\partial\Phi/\partial y$) is greater than the Coriolis force (fu) as seen in Fig. 7b. The generation of a westerly ageostrophic wind in stages 1 and 2 is associated with an increase of the eastward acceleration (Fig. 8a), which is related to the decline in the westward Coriolis force (Fig. 8b) associated with the northward progression of the Atlantic marine ITCZ as discussed above. From mid-July to late September, the ageostrophic wind is in the same direction as the geostrophic wind, as the Coriolis force is larger than the pressure gradient force (Fig. 7b). This occurs as a result of enhanced westerly acceleration by the zonal Coriolis force. As displayed in Fig. 8b, the Coriolis force in the jet acceleration region changes direction from westward to eastward in mid-July, enhancing the westerly flow.

From June to October, the ageostrophic wind component remains steady at about 1 m s^{-1}, so variations in the geostrophic wind explain much of the seasonality of the total zonal wind (Fig. 9). The daily zonal wind speed in the jet averaging region is significantly correlated (at the 95% confidence level) with the meridional geopotential height gradient from 8°–10°N, 15°–24°W, and from 7°–14°N, 24°–32°W in all stages.

The above analysis demonstrates that the WAWJ results from multiscale interactions over the eastern Atlantic. It is also an example of atmosphere–ocean–land surface interaction because its formation is controlled by both continental and ocean processes. When the seasonal development of the continental thermal low is superimposed on the seasonal progression of the marine ITCZ, a region of enhanced eastward acceleration forms off the west coast of Africa. The resulting WAWJ is, therefore, a regional-scale feature controlled by these large-scale structures.

b. Formation of the off shore low

The pressure gradient at 8°–13°N over the eastern Atlantic is critical to the formation of the WAWJ. As revealed in the reanalysis climatology (Fig. 2), the westward extension of the thermal heat low at 925 hPa is associated with the development of an offshore low at 15°N along the West African coast. The formation of the offshore low (Fig. 2c) is investigated in this section.

Figures 10a–e show SSTs (contoured) with wind vectors and geopotential heights (shaded) at 1000 hPa for each stage of the WAWJ development. The wind and geopotential height fields are similar to those at 925 hPa (see Fig. 2), but the relationship with surface heating is more clear at the lower level. Warm SSTs accompanied by low geopotential heights are located near the coast in every stage. In early June, the warmest SSTs are centered between 6°–11°N and 12°–20°W (Fig. 10a). From late June to early September, the region of warmest coastal SSTs moves north (Figs. 10b,c), and low geopotential heights extend westward over the eastern Atlantic at 10°N, reaching to about 28°W in stage 3 (Fig. 10c). Note that the Atlantic cold SST tongue is evident at 6°–10°N in stages 3 and 4 (Figs. 10c,d). During stage 4, the warmest SSTs are located at 14°N, essentially coincident with the coastal low (Fig. 10d). The warmest SSTs extend southwestward from the West African coast to 24°W and 8°N in October, and the low center moves southward to about 8°N (Fig. 10e). Figure 10 suggests that the evolution of the low is associated with heating of the ocean surface, so the surface heat budget is examined.

Figure 11a displays the net surface heating [Eq. (6)] from the ERA-40 reanalysis for stage 3. As shown in Fig. 11a, net heating values over land are smaller than 10 W m^{-2}, but a net surface heating maximum of 130 W m^{-2} is positioned at 17°–23°N over the eastern Atlantic. Near the coast, a net surface cooling maximum of -80 W m^{-2} is located at 13°W and 7°N.

Since the ERA-40 heat balance values contain uncertainty (Allan et al. 2004), we also examined the radiation variables in the NCEP1 reanalysis for 1958–2001 and the satellite-derived variables in the National Aeronautics and Space Administration (NASA)/Global Energy and Water Cycle Experiment (GEWEX) Surface Radiation Budget (SRB; data obtained from the NASA Langley Research Center Atmospheric Sciences Data Center NASA/GEWEX SRB Project) products for 1984–2004. A narrow net surface heating center is found at 14°–25°N, 15°–18°W and near the coast in the NCEP1 climatology. Each component of the heat budget in the NCEP1 reanalysis is similar to the ERA-40 reanalysis (not shown). Surface solar and longwave radiation in the

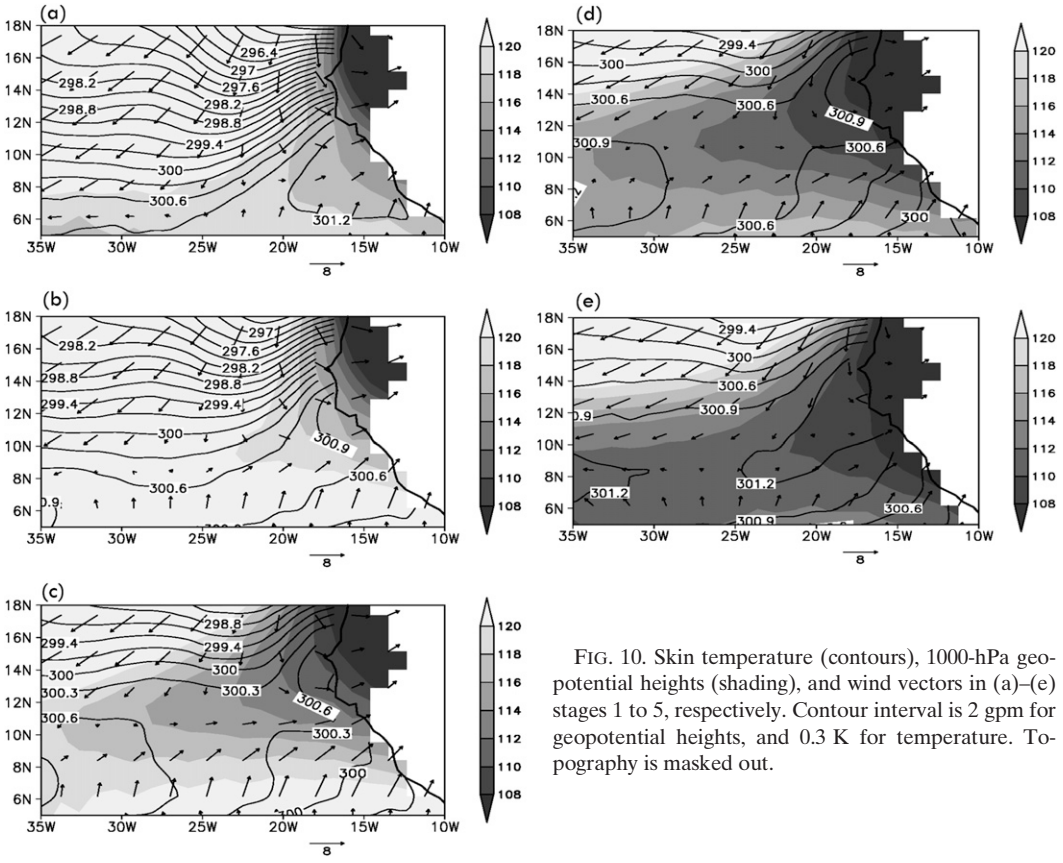

FIG. 10. Skin temperature (contours), 1000-hPa geopotential heights (shading), and wind vectors in (a)–(e) stages 1 to 5, respectively. Contour interval is 2 gpm for geopotential heights, and 0.3 K for temperature. Topography is masked out.

SRB climatology also show features similar to the ERA-40 reanalysis (not shown).

Figure 11b shows the skin temperature differences between stage 3 and stage 2 (stage 3 minus stage 2). Corresponding to the net surface heating rates shown in Fig. 11a, SSTs in stage 3 are about 2 K warmer than in stage 2 at 17°–21°N near the coast, with relatively warm SSTs extending southward to 6°N at 35°W. Consistent with the surface cooling near 7°N, 13°W, SSTs in stage 3 are about 0.5 K cooler than in stage 2 near the western Guinean coast. The pattern of surface heating shown in Fig. 11a, with warming to the north and cooling to the south, moves the coastal SST maximum to the north between stages 2 and 3 (Figs. 10b,c).

Each component of the surface heat budget is examined for the time of the jet maximum (stage 3). Figure 12a displays the net solar radiative heat flux. As shown in Fig. 12a, a solar heating center of 260 W m^{-2} is located at 14°–25°N over the eastern Atlantic (extending northward to about 29°N, not shown). To the south, solar heating rates are much lower, with a minimum of 60 W m^{-2} at 6°–11°N on the coast. So the pattern of surface heating to the north and cooling to the south seen in the net surface heat balance that advances the warm coastal SSTs northward from stage 2 to stage 3 is supported by the net surface solar radiation.

In addition to the distribution of solar heating, the pattern of latent cooling in the eastern Atlantic helps drive the northward shift of the SST maximum off the west coast of Africa. As seen in Fig. 12b, the evaporative cooling of the surface is minimal at 12°–18°N along the coast, and much stronger to the south with a maximum at 2°–7°N.

The net longwave radiative and sensible heat fluxes (not shown) are relatively uniform between 12° and 22°N over the eastern Atlantic, so they do not play a primary role in moving the coast SST maximum to the north between stages 2 and 3. It is the sum of the solar and latent heat fluxes (Figs. 12a,b) that produces the pattern of heating to the north and cooling to the south along the coast shown in Fig. 11a, and that moves the SST maximum northward between stages 2 and 3 of the jet.

An examination of cloud distributions helps relate the surface heating pattern to the movement of the ITCZ and, thereby, the dynamics discussed in the previous section. Figure 13a shows total cloud cover from the ERA-40 climatology (1958–2001) for stage 3. Between 16°–25°N and 15°–24°W, the cloud fraction is 0.4 or lower, allowing relatively high amounts of solar radiation

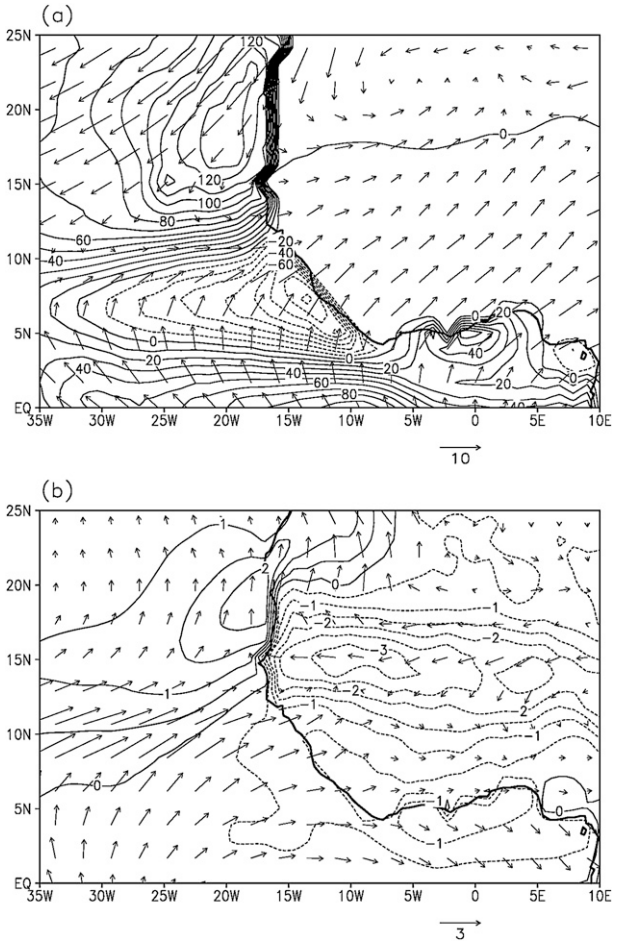

FIG. 11. (a) Net surface heating (W m^{-2}) and 925 hPa wind vectors (m s^{-1}) from the ERA-40 reanalysis during the WAWJ's mature stage (stage 3). (b) Skin temperature (K) and 925-hPa wind differences for (stage 3) − (stage 2). Contour intervals are (a) 10 W m^{-2} and (b) 0.5 K.

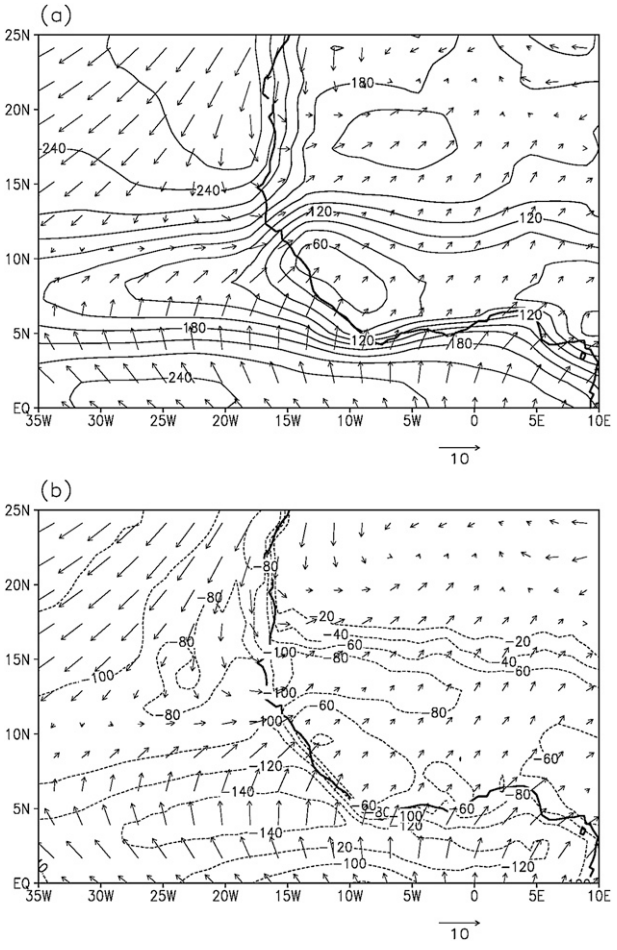

FIG. 12. (a) Downward solar radiation and (b) upward latent heating flux averaged between 22 Jul and 5 Sep for the jet maximum period (W m^{-2}). Positive values denote downward heat flux (surface heating), while negative values denote upward heat flux (surface cooling). Vectors are winds at 10 m. Contour interval is 20 W m^{-2}.

to reach the surface (Fig. 12a). The cloud cover fraction is even lower over the Sahara, but the surface albedo is much higher than over the ocean (0.3–0.4 compared with 0.05–0.1) so the solar heating is centered over the ocean. The low solar heating of the surface at 4°–12°N (Fig. 12a) is related to the higher cloud covers of the ITCZ region (Fig. 13a).

Since cloud cover in the reanalysis is not assimilated, satellite measurements from the International Satellite Cloud Climatology Project (ISCCP; http://isccp.giss.nasa.gov; Rossow and Schiffer 1999) climatology (1984–2007) for August are used to validate the cloud distribution shown in Fig. 13a. As shown in Fig. 13b, the mean cloud cover distribution in the ISCCP climatology is similar to that in the ERA-40 reanalysis, with a minimum between 20° and 25°N on the continent that extends westward over the eastern Atlantic. These low cloud amounts over the coastal eastern Atlantic are related to the low-level inversion (at 17°–25°N, not shown) associated with the westward advection of the dry and warm Saharan air (i.e., the Saharan air layer), which suppresses deep convection (Wong and Dessler 2005). The ISCCP cloud data also confirm the high cloud amounts between 5° and 12°N associated with the ITCZ.

The pattern of latent cooling of the surface (Fig. 12b) is also related to the seasonal movement of the ITCZ through the surface winds. The cooling maximum at 2°–7°N is associated with strong surface winds to the south of the ITCZ, while the minimum in the north is associated with the low wind speeds in the offshore low to the north of the WAWJ. As the offshore low develops, the surface winds weaken and latent heat loss decreases, which tends to warm SSTs and deepen the low.

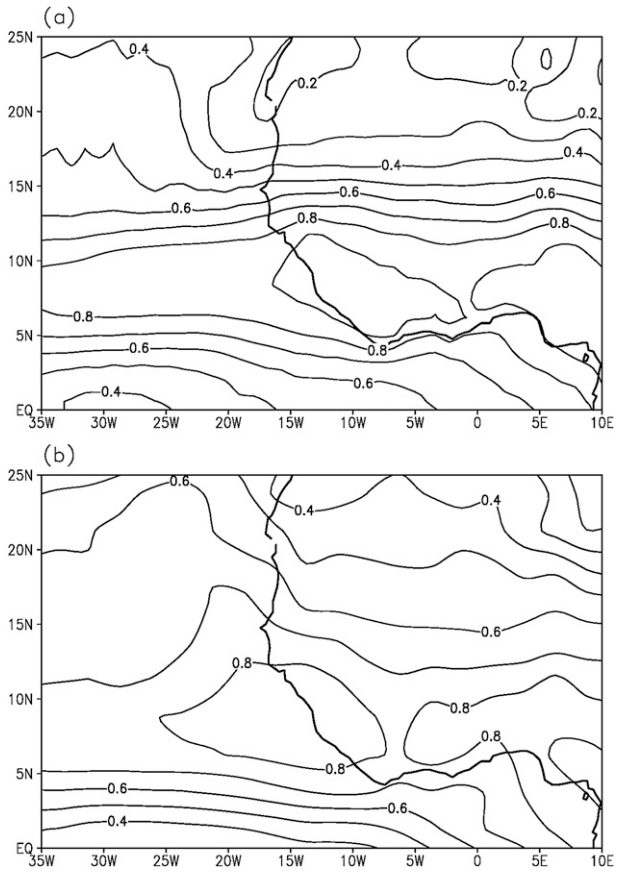

FIG. 13. Total cloud cover (fraction) in (a) the ERA-40 climatology (1958–2001) for the WAWJ mature stage (stage 3) and (b) the ISCCP climatology (1984–2007) for August.

Surface heat budgets in different stages (not shown) reveal a similar association between the net surface heating and SST warming. From early June to mid-October (stages 1–5), the net surface heating center is located at 19°, 20°, 19°, 17°, and 13°N, respectively, with a net cooling center associated with the ITCZ to the south.

Grodsky et al. (2003) also discuss the relationship between the WAWJ and SSTs, demonstrating that the presence of the jets causes a cooling of SSTs through Ekman pumping and latent heat loss. They find that these two processes cool eastern Atlantic SSTs in August by about 0.35 K, when the westerly wind speed is 2 m s^{-1} stronger between a strong jet year (1999) and a weak jet year (2000). This cooling effect is quite local, and has only a small effect on the larger-scale surface heat balances discussed here.

6. Conclusions

The climatology and dynamics of the West African westerly jet (WAWJ) are studied in the relatively high-resolution (about 1.125° latitude by 1.125° longitude) ERA-40 reanalysis. This work builds upon the observational analysis of Grodsky et al. (2003), who first identify the westerly flow onto the continent near 10°N as a jet using QuikSCAT data. The work is further motivated by the results of Patricola and Cook (2007, 2008) who find that the WAWJ plays a crucial role in moisture transport into the Sahel, and that the jet can vary independently of the southwesterly monsoon flow. Here we show that the structure and dynamics of the WAWJ and the southwesterly monsoon flow are distinct and study the processes that cause the jet to form.

The WAWJ develops at the beginning of June, reaches a maximum intensity of 6 m s^{-1} at 925 hPa during August, and dissipates in mid-October. Based on the strength of the zonal wind speed in the ERA-40 climatology (1958–2001), five stages of jet development are identified. At its mature stage, 22 July–5 September, the jet extends between 8°–11°N and 12°–30°W, and from the surface to 700 hPa.

In the 6-hourly ERA-40 reanalysis, the jet displays a weak semidiurnal cycle, with two wind speed maxima of 5–6 m s^{-1} at 0500 and 1700 local time and minima of 4–5 m s^{-1} at 1100 and 2300 local time.

The formation of the WAWJ depends on multiscale interactions. Over the eastern Atlantic, a region of enhanced westerly acceleration forms when the seasonal progression of the continental low is superimposed on the seasonal progression of the Atlantic marine ITCZ. While the pressure gradient force in the relatively small region between 9°–10°N and 20°–30°W accelerates the zonal wind to the east, the superposition of the large-scale meridional convergence associated with the ITCZ constrains the development of meridional acceleration. In this way, the regional-scale WAWJ is coupled to large-scale processes.

Analysis of the momentum budget shows that the mature WAWJ is supergeostrophic. A westerly ageostrophic wind component develops as the southerly flow adds to eastward acceleration via the Coriolis term. The ageostrophic wind contributes up to 40% of the total wind during stage 2 and stage 4, for example, in mid-July and from early to mid-September.

The geostrophic zonal wind explains much of the WAWJ's seasonal variation. The meridional pressure gradient at 8°–13°N associated with the geostrophic wind is influenced by the westward extension of the continental thermal low, which in the ERA-40 reanalysis is related to the formation of an offshore low over the eastern Atlantic.

The surface heat budget analysis reveals that the development of the offshore low is related to seasonal SST warming in the eastern Atlantic, a response to the net surface heating. From early June to mid-October, a net

surface heating pattern with warming at 8°–25°N and cooling to the south at 4°–8°N persists over the eastern Atlantic between 10° and 35°W. As the magnitude of this heating pattern varies, SSTs between 6° and 18°N vary, with a coastal SST maximum moving northward and southward. The offshore low at 1000 hPa is collocated with this coastal SST maximum. In stage 3, when coastal SSTs strongly warm and the thermal low is deep, the westward extension of the low reaches its maximum, with the strongest southward geopotential height gradient setting up in the jet region.

The net surface heat pattern mainly reflects the distribution of the solar radiative and latent heat fluxes. The solar radiation maximum over the eastern Atlantic is associated with low cloud amounts at 16°–25°N in the coastal region where there is a low-level inversion that prohibits strong convection (Wong and Dessler 2005), and the minimum to the south is related to high cloud amounts in the ITCZ. The weak surface wind speeds in the offshore low and strong wind speeds to the south of the ITCZ are associated with the latent cooling minimum to the north and maximum to the south, respectively.

In summary, the Atlantic ITCZ plays an important role in the WAWJ formation. The ITCZ favors formation of a purely westerly acceleration zone, and thus is dynamically associated with the jet formation. The ITCZ is also thermally related to the WAWJ formation through the surface heat budget and the formation of the offshore low.

Previous studies discuss the importance of westerly flow over the eastern Atlantic and West Africa without distinguishing the WAWJ from the southwesterly monsoon flow. Here we demonstrate that the WAWJ is a feature distinct from the monsoon flow.

First, the geographical locations of the two are different. The WAWJ is located over the eastern Atlantic and the West African coast, while the monsoon westerlies are mainly over the West African continent. In the summer, the jet is centered between 8°N and 11°N (Figs. 1a and 3a), and the monsoon westerlies extend inland to 20°N (Figs. 1a and 3b).

The vertical wind in the jet region is up to 10 times greater than that in the monsoon region from late July to early September. While the meridional wind in the monsoon region is 2–3 m s^{-1} stronger than in the WAWJ region, the maximum zonal wind is about 2 m s^{-1} weaker (Fig. 5). The diurnal cycle of the monsoon westerly flow, which has a peak at 0600 local time and a minimum at 1800 local time, is also distinguished from the semidiurnal cycle of the WAWJ (Fig. 4).

The monsoon dynamics is also different from that of the WAWJ. In the monsoon region, momentum balance is achieved among the pressure gradient force, Coriolis force, and a strong friction term, and the flow is subgeostrophic. The formation of the West African monsoon is essentially related to the heat capacity differences between the West African continent and the Atlantic, which is associated with large-scale land–sea pressure gradients at low levels and the seasonal migration of the southerly trades. Thus, the monsoon development is directly related to the strength of the continental thermal low, and both peak earlier in the year than the WAWJ (Fig. 2b and Fig. 5b). In contrast, the WAWJ is more closely related to the westward extension of the thermal low as well as the seasonal progression of the marine ITCZ over the eastern Atlantic.

Considering the important role of the WAWJ in moisture transport, further investigation of how the WAWJ is related to low-level moisture convergence and Sahel precipitation on interannual and decadal scales will be addressed in a subsequent paper.

Acknowledgments. The authors would like to acknowledge the invaluable support of Dr. E. K. Vizy in providing analysis tools for this study and comments on the manuscript. Dr. Sumant Nigam and an anonymous reviewer provided insightful and constructive suggestions that improved the paper, as did our colleagues at UT Austin and Cornell, Dr. C. M. Patricola, E. E. Riddle, and Prof. S. J. Colucci. Financial support was provided by DOE's Abrupt Climate Change Program.

REFERENCES

Allan, R. P., M. A. Ringer, J. A. Pamment, and A. Slingo, 2004: Simulation of the Earth's radiation budget by the European Center for Medium-Range Weather Forecasts 40-year reanalysis (ERA40). *J. Geophys. Res.,* **109,** D18107, doi:10.1029/2004JD004816.

Braconnot, P., S. Joussaume, N. de Noblet, and G. Ramstein, 2000: Mid-Holocene and last glacial maximum African monsoon changes as simulated within the Paleoclimate Modeling Intercomparison Project. *Global Planet. Change,* **26,** 51–66.

Cadet, D. L., and N. O. Nnoli, 1987: Water vapor transport over Africa and the Atlantic Ocean during summer 1979. *Quart. J. Roy. Meteor. Soc.,* **113,** 581–602.

Cook, K. H., 1999: Generation of the African easterly jet and its role in determining West African precipitation. *J. Climate,* **12,** 1165–1184.

Druyan, L. M., and R. D. Koster, 1989: Sources of Sahel precipitation for simulated drought and rainy seasons. *J. Climate,* **2,** 1438–1446.

Fontaine, B., P. Roucou, and S. Trzaska, 2003: Atmospheric water cycle and moisture fluxes in the West African monsoon: Mean annual cycles and relationship using NCEP/NCAR reanalysis. *Geophys. Res. Lett.,* **30,** 1117, doi:10.1029/2002GL015834.

Grist, J. P., and S. E. Nicholson, 2001: A study of the dynamic factors influencing the rainfall variability in the West African Sahel. *J. Climate,* **14,** 1337–1359.

Grodsky, S. A., J. A. Carton, and S. Nigam, 2003: Near surface westerly wind jet in the Atlantic ITCZ. *Geophys. Res. Lett.,* **30,** 2009, doi:10.1029/2003GL017867.

Gu, G., and R. F. Adler, 2004: Seasonal evolution and variability associated with the West African monsoon system. *J. Climate,* **17,** 3364–3377.

Hagos, S. M., and K. H. Cook, 2005: Influence of surface processes over Africa on the Atlantic marine ITCZ and South American precipitation. *J. Climate,* **18,** 4993–5010.

——, and ——, 2008: Ocean warming and late twentieth-century Sahel drought and recovery. *J. Climate,* **21,** 3797–3814.

Jury, M. R., D. B. Enfield, and J.-L. Melice, 2002: Tropical monsoons around Africa: Stability of El Niño–Southern Oscillation associations and links with continental climate. *J. Geophys. Res.,* **107,** 3151, doi:10.1029/2000JC000507.

Kalnay, E., and Coauthors, 1996: The NCEP/NCAR 40-Year Reanalysis Project. *Bull. Amer. Meteor. Soc.,* **77,** 437–471.

Kanamitsu, M., W. Ebisuzaki, J. Woollen, S. Yang, J. Hnilo, M. Fiorino, and G. Potter, 2002: NCEP–DOE AMIP-II Reanalysis (R-2). *Bull. Amer. Meteor. Soc.,* **83,** 1631–1643.

Koster, R. J., Jouzel, R. Suozzo, G. Russell, W. Broecker, D. Rind, and P. Eagleson, 1986: Global source of local precipitation as determined by the NASA/GISS GCM. *Geophys. Res. Lett.,* **13,** 121–124.

Lamb, P. J., 1983: West African water vapor variations between recent contrasting sub-Saharan rainy seasons. *Tellus,* **35A,** 198–212.

Nicholson, S. E., and J. P. Grist, 2003: The seasonal evolution of the atmospheric circulation over West Africa and equatorial Africa. *J. Climate,* **16,** 1013–1030.

Patricola, C. M., and K. H. Cook, 2007: Dynamics of the West African monsoon under mid-Holocene processional forcing: Regional climate model simulations. *J. Climate,* **20,** 694–716.

——, and ——, 2008: Atmosphere/vegetation feedbacks: A mechanism for abrupt climate change over northern Africa. *J. Geophys. Res.,* **113,** D18102, doi:10.1029/2007JD009608.

Rossow, W. B., and R. A. Schiffer, 1999: Advances in understanding clouds from ISCCP. *Bull. Amer. Meteor. Soc.,* **80,** 2261–2288.

Sijikumar, S., P. Roucou, and B. Fontaine, 2006: Monsoon onset over Sudan-Sahel: Simulation by the regional scale model MM5. *Geophys. Res. Lett.,* **33,** L03814, doi:10.1029/2005GL024819.

Simmons, A., S. Uppala, and D. Dee, 2007a: Update on ERA-Interim. *ECMWF Newsletter,* No. 111, ECMWF, 5.

——, ——, ——, and S. Kobayashi, 2007b: ERA-Interim: New ECMWF reanalysis products from 1989 onwards. *ECMWF Newsletter,* No. 110, ECMWF, 25–35.

Tomas, R. A., and P. J. Webster, 1997: The role of inertial instability in determining the location and strength of near-equatorial convection. *Quart. J. Roy. Meteor. Soc.,* **123,** 1445–1482.

Uppala, S. M., and Coauthors, 2005: The ERA-40 Re-Analysis. *Quart. J. Roy. Meteor. Soc.,* **131,** 2961–3012.

Wong, S., and A. E. Dessler, 2005: Suppression of deep convection over the tropical North Atlantic by the Saharan air layer. *Geophys. Res. Lett.,* **32,** L09808, doi:10.1029/2004GL022295.